Spinal microgliosis due to resident microglial proliferation is required for pain hypersensitivity after peripheral nerve injury

Nan Gu, Jiyun Pen, Madhuvika Murugan, Xi Wang, Ukpong B. Eyo, Dongming Sun, Yi Ren, Emanuel DiCicco-Bloom, Wise Young, Hailong Dong, Long-Jun Wu

Supplemental Information

Supplemental Figure 1-6

Supplemental Movie 1

Supplemental Experimental Procedures

Supplemental References

Supplemental Figure 1-6

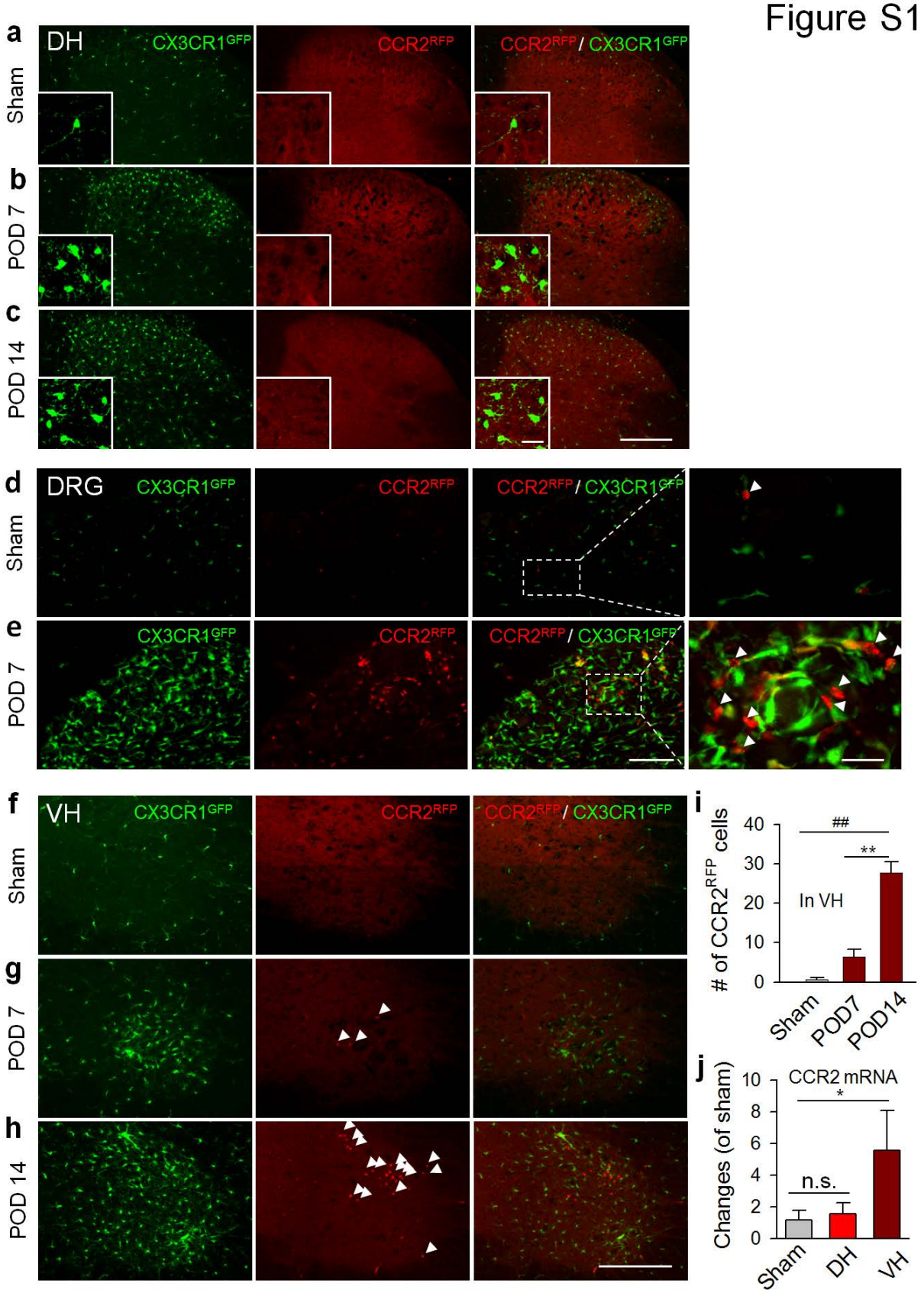

Figure S1 (related to Figure 1). Monocytes do not infiltrate into the dorsal horn, but into DRG and the ventral horn, in CCR2$^{RFP/+}$:CX3CR1$^{GFP/+}$ mice after SNT.

(**a-c**) Representative confocal images of the ipsilateral spinal dorsal horn (DH) in sham **(a)**, POD 7 (**b**) and POD 14 (**c**) following SNT in double transgenic CCR2$^{RFP/+}$:CX3CR1$^{GFP/+}$ mice (n = 4 mice per group). Resident GFP^{+} microglia are shown in green. There are no red infiltrated hematogenous RFP^{+} monocytes under all conditions. Scale bar is 200 μm.

(**d-e**) Representative confocal images of the ipsilateral dorsal root ganglia (DRG) in sham (**d**) and POD 7 (**e**) with corresponding higher magnification images of the boxed regions following SNT in double transgenic CCR2$^{RFP/+}$:CX3CR1$^{GFP/+}$ mice (n = 4 mice per group). Scale bar is 100 μm and 25 μm for lower and higher magnification images, respectively. There are a lot of infiltrated RFP^{+} monocytes in the DRG (arrowheads).

(f-h) Representative confocal images of the ipsilateral spinal cord ventral horn (VH) in sham **(f)**, POD 7 **(g)** and POD 14 **(h)** following SNT in double transgenic CCR2$^{RFP/+}$:CX3CR1$^{GFP/+}$ mice. Arrowheads indicate CCR2^{RFP} monocytes. Scale bar is 200 μm (n = 3 mice per group).

(i) Summarized data for the number of CCR2$^{RFP/+}$ cells in the VH in sham, POD 7 and POD 14 after SNT (n = 3 mice for each group; 3-5 sections/mice). The number of RFP^{+} monocytes increases in the VH with time. Data are presented as mean ± s.e.m; $^{\#\#}$P < 0.01 compared with sham; **P < 0.01 compared with POD 7.

(j) Upregulation of CCR2 mRNA occurs in the VH but not the DH at POD 7 after SNT or in sham control (n = 4-5 mice per group). Data are presented as mean ± s.e.m; *P < 0.05 compared with sham (fold changes of sham).

Figure S2

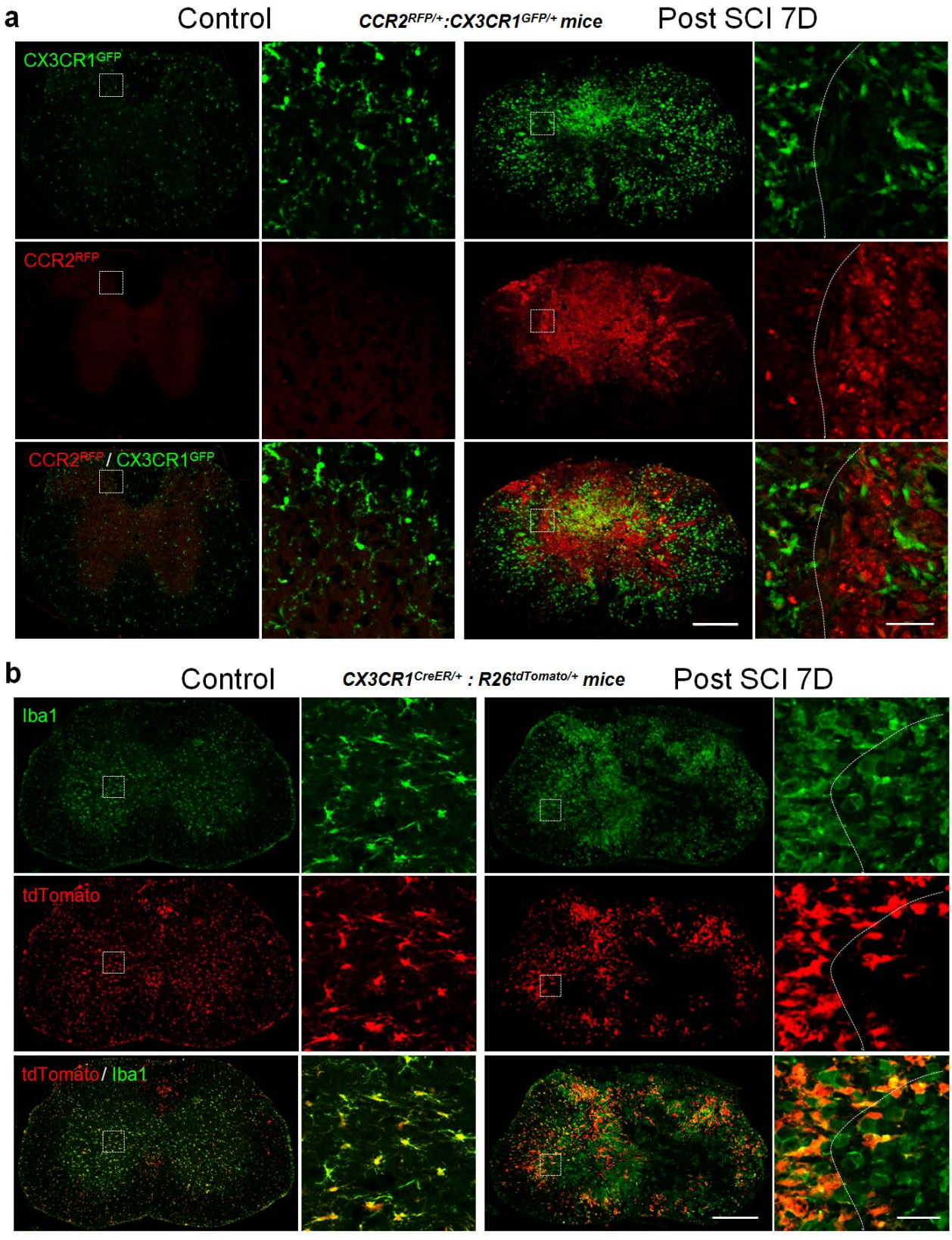
a
Control
CCR2RFP/+:CX3CR1GFP/+ mice
Post SCI 7D
CX3CR1GFP
CCR2RFP
CCR2RFP / CX3CR1GFP
b
Control
CX3CR1CreER/+ : R26tdTomato/+ mice
Post SCI 7D
Iba1
tdTomato
tdTomato / Iba1

Figure S2 (related to Figure 1). Monocyte infiltration in CCR2$^{RFP/+}$:CX3CR1$^{GFP/+}$ mice and CX3CR1$^{creER/+}$: R26$^{tdTomato/+}$ reporter mice after T10 spinal cord injury. **(a-b)** Representative confocal images of the T10 spinal cord in sham control and 7 days following spinal cord injury (SCI) in double transgenic CCR2$^{RFP/+}$:CX3CR1$^{GFP/+}$ mice (**a**, n = 3 mice for sham and 5 for injury group) and CX3CR1$^{creER/+}$: R26$^{tdTomato/+}$ reporter mice (**b**, n = 4 mice per group). Dotted box shows region of high power image. **(a)** Numerous CCR2$^{RFP/+}$ monocytes were found around and inside the damage core (Dotted line shows the boundary of the damaged core). **(b)** Resident microglia are tdTomato^{+}Iba1^{+} cells and infiltrated hematogenous monocytes are tdTomato^{-}Iba1^{+} cells**.** Note the numerous tdTomato^{-}Iba1^{+} cells that localize around and inside the damage core, which is delineated by dotted lines. Scale bar is 300 μm and 50 μm for lower and higher magnification images, respectively.

Figure S3

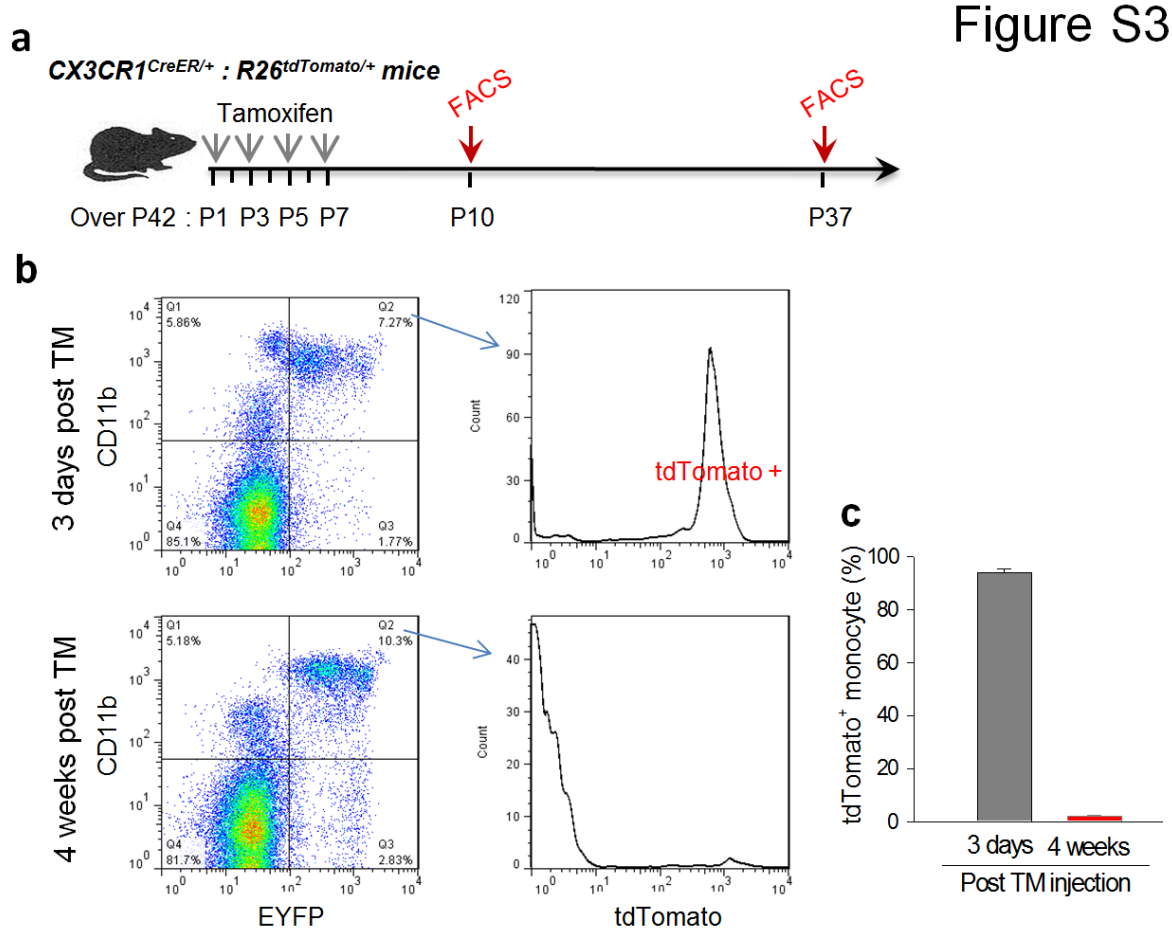
a
CX3CR1CreER/+ : R26tdTomato/+ mice
Tamoxifen
FACS
FACS
Over P42 : P1 P3 P5 P7
P10
P37
b
3 days post TM
4 weeks post TM
CD11b
EYFP
tdTomato
tdTomato +
Count
Q1 5.86%
Q2 7.27%
Q4 85.1%
Q3 1.77%
Q1 5.18%
Q2 10.3%
Q4 81.7%
Q3 2.83%
c
tdTomato+ monocyte (%)
3 days
4 weeks
Post TM injection

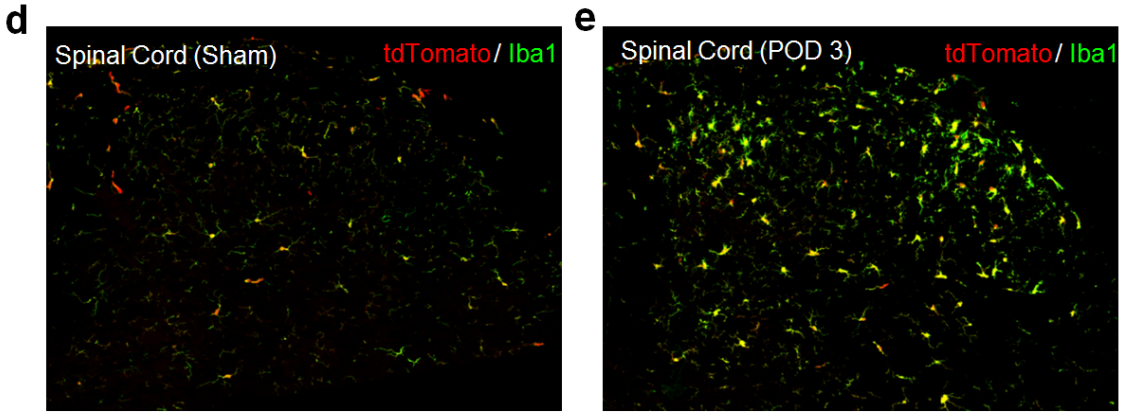
d
Spinal Cord (Sham)
tdTomato / Iba1
e
Spinal Cord (POD 3)
tdTomato / Iba1

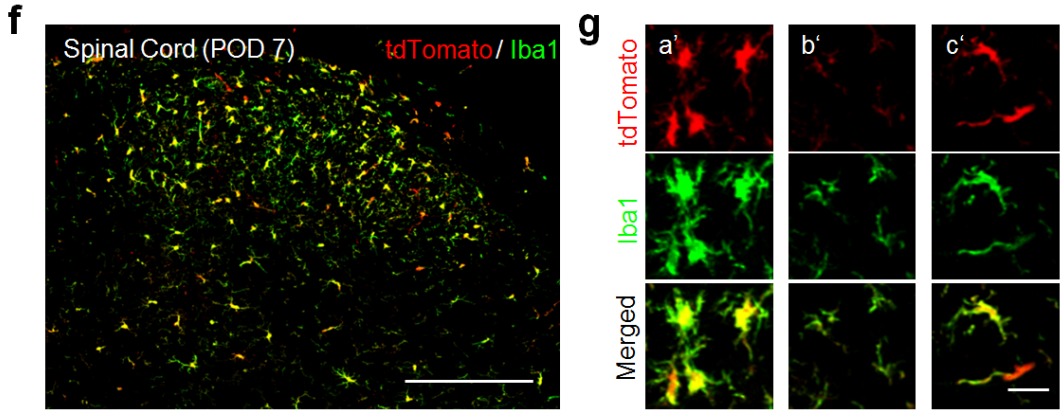
f
Spinal Cord (POD 7)
tdTomato / Iba1
g
tdTomato
Iba1
Merged
a'
b'
c'

Figure S3 (related to Figure 1). No monocyte infiltration into the dorsal horn of the spinal cord in CX3CR1$^{CreER/+}$:R26$^{tdTomato/+}$ reporter mice at POD3 and POD7 after SNT.

(a-c) Blood flow cytometric analysis of CX3CR1$^{creER/+}$: R26$^{tdTomato/+}$ reporter mice after Tamoxifen (TM) treatment. **(a)** Schematic time-line for intraperitoneal TM administration and flow cytometric analysis (FACS). **(b)** Representative examples of blood flow cytometric analysis of peripheral CD11b^{+} tdTomato^{+} monocytes in the blood at 3 days and 4 weeks after the last TM administration. Note that CD11b^{+} CX3CR1^{EYFP+} monocytes were largely tdTomato negative. **(c)** Bar graph showing the results of the FACS analysis (n = 3 mice; bars represent mean ± s.e.m. counts) of CD11b^{+} tdTomato^{+} cells in the blood. tdTomato^{+} cells were mostly turnover in 4 weeks after TM treatment compared those with 3 days after TM treatment.

(d-g) Representative confocal images of Iba1 staining showing all spinal DH microglia (Iba1) were RFP (tdTomato) positive in sham **(d)**, POD3 **(e)** and POD7 **(f)** after SNT in CX3CR1$^{CreER/+}$/R26$^{tdTomato/+}$ mice with 4 week interval between tamoxifen injection and immunostaining (n = 4 mice per group). Scale bar is 200 µm. **(g)** Representative higher magnification images showing that all cells are both Iba1^{+} and tdTomato^{+}, most cells have both strong Iba1 and tdTomato signal (a'), while some of them have weaker tdTomato signal (b') or have tdTomato signal seen in processes(c'). Scale bar is 20 µm.

Figure S4

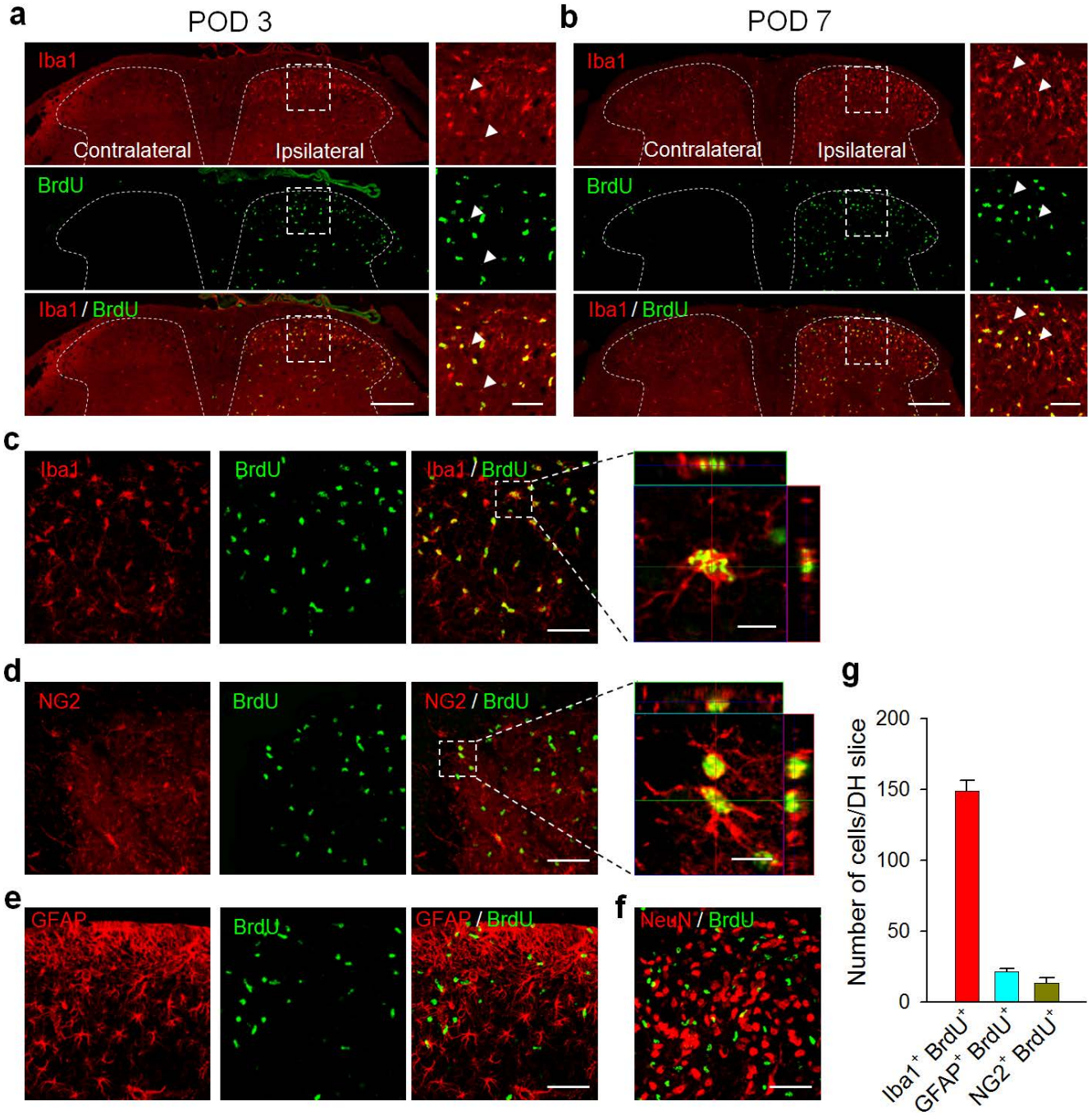
a
POD 3
Iba1
Contralateral
Ipsilateral
BrdU
Iba1 / BrdU
b
POD 7
Iba1
Contralateral
Ipsilateral
BrdU
Iba1 / BrdU
c
Iba1
BrdU
Iba1 / BrdU
d
NG2
BrdU
NG2 / BrdU
e
GFAP
BrdU
GFAP / BrdU
f
NeuN / BrdU
g
Number of cells/DH slice
200
150
100
50
0
Iba1+ BrdU+
GFAP+ BrdU+
NG2+ BrdU+

Figure S4 (related to Figure 3). Local microglial proliferation provides a sustainable source for microgliosis after peripheral nerve injury.

(a-b) Double staining showing co-localization of BrdU (green) and Iba1 (red) in spinal cord DH at POD 3 (**a**) and 7 (**b**) following SNT (n = 4 mice per group). Dotted box shows the region of higher magnification. Most $Iba1^+$ cells are also $BrdU^+$ in the ipsilateral DH while very few $BrdU^+$ cells are present on the contralateral side. Arrowheads indicate some weak but clearly observable BrdU signals colocalized with Iba1 staining; these cells were counted as $BrdU^+Iba1^+$ microglia. Scale bar is 200 μm and 50 μm for lower and higher magnification images, respectively.

(c-g) Most of the proliferation events occurred in microglia but not in astrocytes, NG2 cells, or neurons after SNT. (**c**) Representative confocal images showing double staining of co-localized BrdU (green) and Iba1 (red) in the spinal cord DH at POD 7 following SNT (n = 4 mice). The region of high magnification z-sectioned image shows that the $BrdU^+$ signal is located in the nuclei of $Iba1^+$ microglia. Scale bar is 50 μm and 10 μm for lower and higher magnification images. (**d**-**e**) Double staining showing co-localization of BrdU (green) with NG2 (red in **d**) or GFAP (red in **e**) in the DH at POD 7 following SNT (n=3-5 mice). Note there is a small percentage of $BrdU^+/NG2^+$ cells (**d**) and $BrdU^+/GFAP^+$ astrocytes (**e**). Dotted box shows region of high magnification z-sectioned image, showing that the BrdU+ signals are also located in the nuclei of $NG2^+$ cells. Scale bar is 50 μm and 10 μm for lower and higher magnification images. **(f)** No co-localization of BrdU (green) and NeuN (red) in the DH at POD 7 after SNT (n=3 mice). **(g)** Quantification of the number of $Iba1^+BrdU^+$, $NG2^+BrdU^+$, and $GFAP^+BrdU^+$ cells in the DH at POD7 after SNT (n = 3–5 mice). Data are presented as mean ± s.e.m.

Figure S5

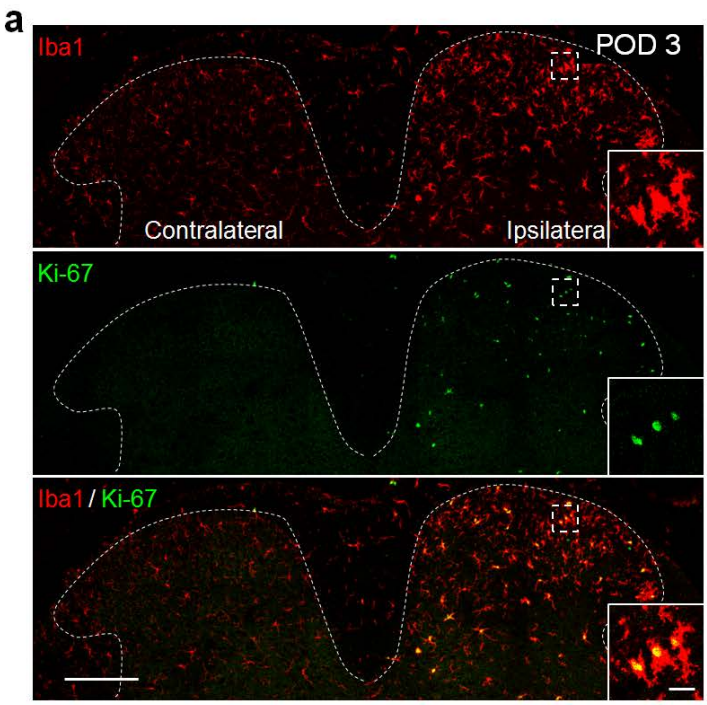
a
Iba1
POD 3
Contralateral
Ipsilatera
Ki-67
Iba1 / Ki-67

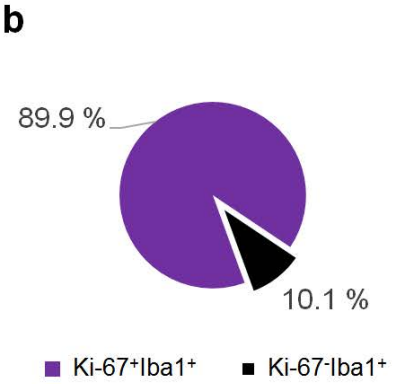
b
89.9 %
10.1 %
Ki-67+Iba1+
Ki-67-Iba1+

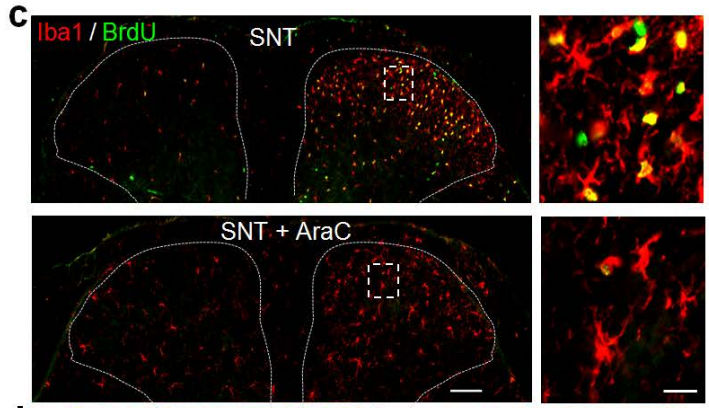
c
Iba1 / BrdU
SNT
SNT + AraC

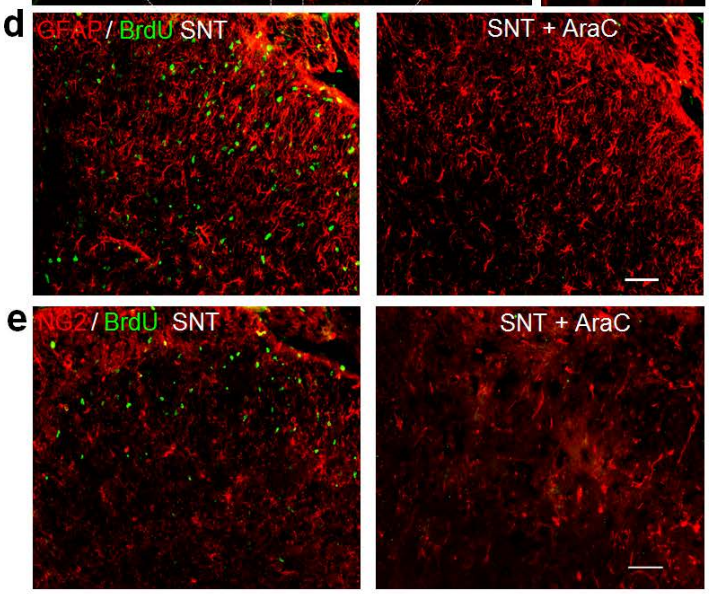
d
GFAP / BrdU SNT
SNT + AraC
e
NG2 / BrdU SNT
SNT + AraC

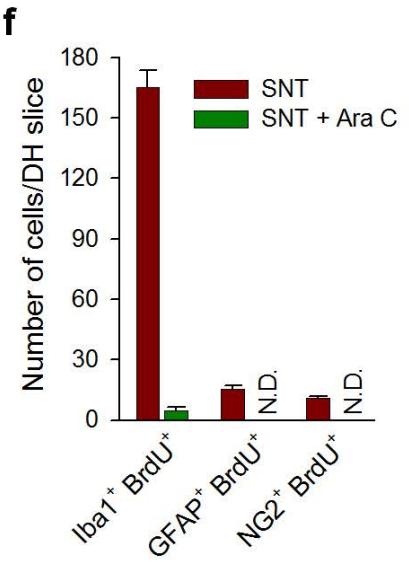
f
Number of cells/DH slice
180
150
120
90
60
30
0
SNT
SNT + Ara C
N.D.
N.D.
Iba1+ BrdU+
GFAP+ BrdU+
NG2+ BrdU+

Figure S5 (related to Figure 4 and 5). Microglial proliferation using Ki-67 labeling and AraC inhibits SNT-induced cell proliferation.

(**a-b, related to Figure 4**) Ki-67 expression in $Iba1^+$ microglia in the dorsal horn at POD 3 after SNT. **(a)** Representative confocal images showing co-localization of Ki-67 (green) and Iba1 (red) in spinal cord DH at POD 3 after SNT (n=6 mice). Insets are high magnification image, showing that $Ki\text{-}67^+$ signal are located in the nuclei of $Iba1^+$ microglia. Scale bar is 200 μm and 20 μm for lower and higher magnification images, respectively. (**b**) A pie chart showing the percentage of $Ki\text{-}67^+$ $Iba1^+$ cells among total $Iba1^+$ cells at POD 3 after SNT (n = 6 mice). Data are presented as mean.

(**c-f, related to Figure 5**) AraC inhibited SNT-induced cell proliferation. AraC (50ug in 5μl ACSF, twice/day at POD1-4 and then once/day at POD5-7) and BrdU (100 mg/kg, i.p. twice daily from POD0 to POD6) were given to the Sham or SNT mice to examine the effect of AraC on SNT-induced cell proliferation. **(c)** Double immunostaining results showed that $BrdU^+Iba1^+$ microglia cells in the ipsilateral dorsal horn were reduced in the AraC group. (**d-e**) Although very few $GFAP^+BrdU^+$ astrocytes (**d**) or $NG2^+BrdU^+$ cells (**e**) were detected, AraC was effective in inhibiting total BrdU cell labeling. Scale bar is 100 μm (**c,** left), 20 μm (**c,** right), and 50 μm (**d**-**e**), respectively. (**f**) Quantitative summary of the number of $Iba1^+BrdU^+$, $NG2^+BrdU^+$, and $GFAP^+BrdU^+$ cells in spinal DH at POD7 after SNT with and without AraC treatment (n = 3 mice). N.D., not detectable. Data are presented as mean ± s.e.m.

Figure S6

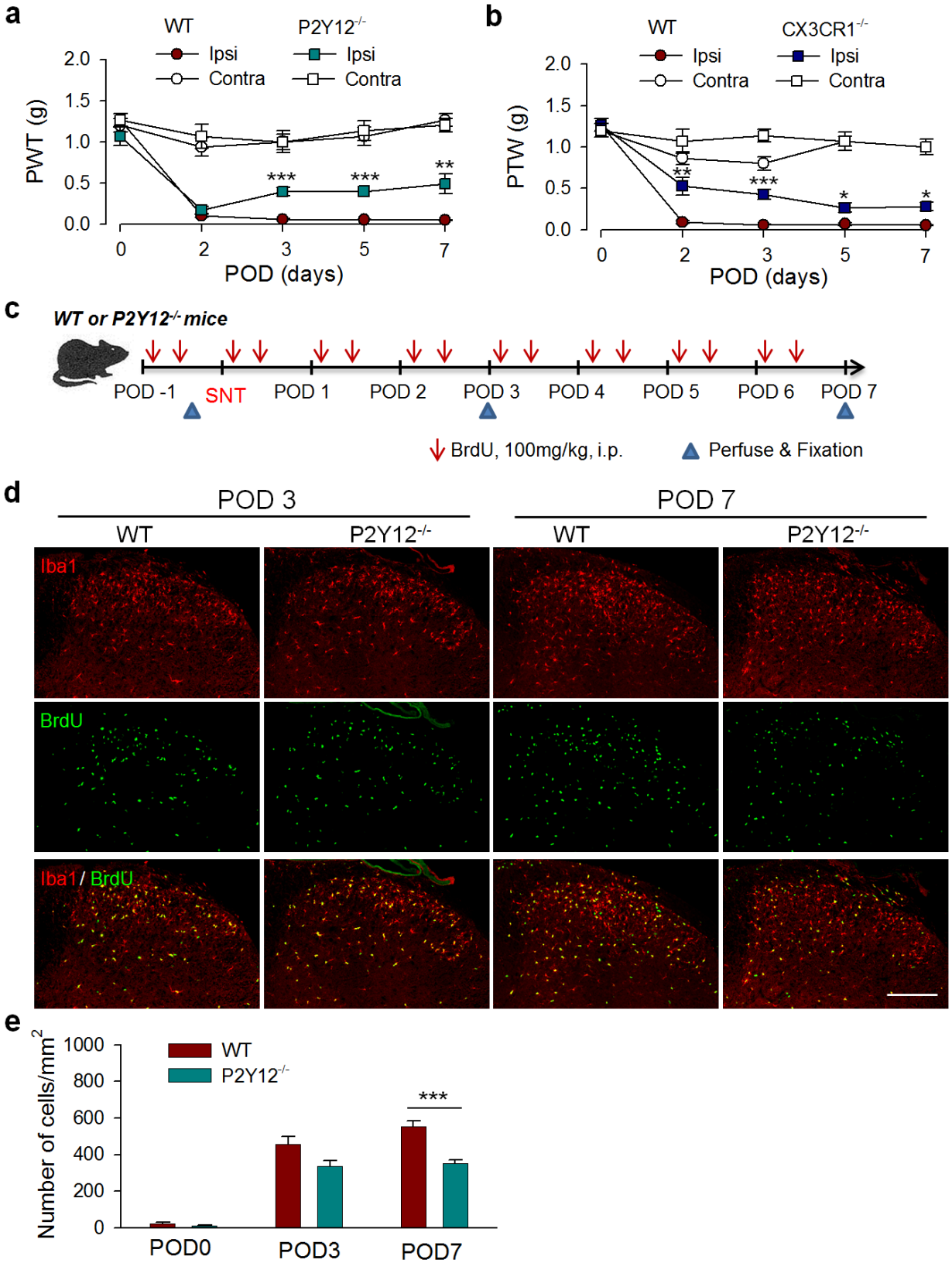
a
WT
P2Y12-/-
Ipsi
Contra
PWT (g)
POD (days)
b
WT
CX3CR1-/-
PTW (g)
c
WT or P2Y12-/- mice
POD -1
SNT
POD 1
POD 2
POD 3
POD 4
POD 5
POD 6
POD 7
BrdU, 100mg/kg, i.p.
Perfuse & Fixation
d
POD 3
POD 7
Iba1
BrdU
Iba1 / BrdU
e
Number of cells/mm2
POD0
POD3
POD7

Figure S6 (related to Figure 5). Neuropathic pain hypersensitivities are attenuated in P2Y12$^{-/-}$ and CX3CR1$^{-/-}$ mice after SNT and correspond to altered microglial proliferation

(**a-b)** Behavioral assays showing that mechanical allodynia in both P2Y12$^{-/-}$ **(a)** and CX3CR1$^{-/-}$ mice **(b)** are reduced compared with WT mice after SNT. Data are shown as mean ± s.e.m. (n = 6 for each group). Repeated measures ANOVA revealed a significant group x repeated measures interaction: F (4, 100) = 30.7; p<0.001 (P2Y12$^{-/-}$ vs. WT). F (4, 100) = 44.6; p<0.001 (CX3CR1$^{-/-}$ vs. WT). *p < 0.05, **p < 0.01, ***p < 0.001 compared with corresponding WT mice by Student's t-test, 2 tail.

(**c-e)** Significantly decreased proliferation of microglia in P2Y12$^{-/-}$ mice after SNT. (**c**) Schematic timeline for BrdU intraperitoneal administration and tissue fixation. (**d**) Representative confocal images of double staining showing co-localization of BrdU (green) and Iba1 (red) in WT and P2Y12$^{-/-}$ spinal cord dorsal horn at POD 3 and 7 following SNT (n = 4-6 mice per group). Scale bar is 200 μm. (**e**) The cumulative decreases of BrdU^{+}Iba1^{+} cells starts at POD3 (p = 0.06) and reaches significance at POD7 (p < 0.001) in P2Y12$^{-/-}$ mice after SNT, compared with those in WT mice. Shown is the summarized data for the number of BrdU^{+} Iba1^{+} cell per mm^{2} in WT and P2Y12$^{-/-}$ mice (n = 4–6 mice in each group per time point). Data are presented as mean ± s.e.m. ***p<0.001 compared with corresponding WT mice by t-test, 2 tail.

Supplementary Movie 1 (related to Figure 4)

Two photon imaging of microglial proliferation in spinal dorsal horn after SNT.

Local microglia proliferation in dorsal horn was directly monitored under 2-photon microscope. Time-lapse movie of microglial cell proliferation was obtained in acute spinal cord slices of CX3CR1$^{GFP/+}$ mice at POD3 after SNT. Arrows denote the dividing microglial cells with parent (white arrow) and daughter cells (red arrow). Time shown in this movie is presented as hr:min. The movie is 180 min long.

Supplemental Experimental Procedures

Mouse Model of Spinal Cord Contusion Injury

Male mice (6–8 weeks old) were used for spinal injury experiments. Spinal cord contusion injuries were inflicted using a modified impactor as described previously (Hashimoto et al., 2007; Wang et al., 2015). Briefly, the spinal cord was exposed by laminectomy at T10 after anesthesia using 2% isoflurane in 0.5 L/min oxygen. The exposed dorsal surface of the spinal cord was subjected to a 5g weight drop with tip diameter of 0.5-mm flat surface from a height of 6.25 mm using a modified NYU impactor. Subsequently, animals were monitored with bladder decompression twice a day until leg movements returned. Mice contused with nonsymmetrical injury were excluded from experimental analysis.

Monocyte Flow Cytometry

Whole mouse blood was collected and monocytes were separated from erythrocytes

and granulocytes on a Ficoll (GE Healthcare) gradient. Separated monocytes were washed with Hank's Balanced Salt Solution and then incubated with 2% goat serum for 10 min, and stained with APC-conjugated CD11b antibody (1:200, Biolegend) for 45 min. Cells were then fixed with 1% paraformaldehyde for 10 min before flow cytometry. Cells were analyzed on a FACSCalibur cytometer (Becton Dickinson) using the CellQuest software (Becton Dickinson).

Pain Behavioral Tests

Mice were previously acclimated to the environment and the experimenter on three consecutive days just before the SNT or sham operation. The tests were performed in a quiet temperature-controlled (23 ± 1 °C) room between the hours of 9:00 and 12:00 noon on days before and 1-7 days after the surgery as described previously (Gu et al., 2015). The experimenter was blinded to the group allocation of the mice under test.

Mechanical allodynia was determined by measuring the incidence of the foot withdrawal in response to mechanical indentation of the plantar surface of each hind paw with a sharp, cylindrical probe with a uniform tip diameter of approximately 0.2 mm provided by a set of Von Frey filaments (0.04 – 2g; North Coast medical Inc.) using a protocol similar to that described previously (Gu et al., 2012). In brief, the mouse was placed on a metal mesh floor and covered with a transparent plastic dome (10 X 15 X 15 cm). The animal rested quietly in this situation after a few (~15) minutes of exploration. The filament was applied from underneath the metal mesh floor to the plantar surface of the foot. The duration of each stimulus was 3 s, in the absence of withdrawal, and the inter-stimulus interval was 10-15 s. The incidence of foot withdrawal

was expressed as a percentage of the 10 applications of each stimulus as a function of force. Fifty percent withdrawal threshold values were determined.

Thermal hyperalgesia was assessed by measuring foot withdrawal latency to heat stimulation, using a protocol described previously (Gu et al., 2012). An analgesia meter (Model 336TG, IITC Life Science Inc.) was used as the heat source. In brief, each mouse was placed in a box containing a smooth, temperature-controlled glass floor (30°C) and allowed to habituate for 20 min. The heat source was focused on a portion of the hind paw, which was flush against the glass, and a radiant thermal stimulus was delivered to that site. The stimulus shut off when the hind paw moved (or after 6s to prevent tissue damage). The intensity of the heat stimulus was maintained constant throughout all experiments. The elicited paw movement occurred at latency between 2.5 and 4s in control animals. Thermal stimuli were delivered four times to each hind paw at 5 to 6 min intervals.

Immunohistochemistry

Mice were deeply anesthetized with isoflurane (5% in O_2) and perfused transcardially with 30 ml PBS followed by 30 ml of cold 4% paraformaldehyde in PBS containing 1.5% picric acid. The target tissues were removed and post-fixed with the same 4% paraformaldehyde overnight at 4°C. The samples were then transferred to 30% sucrose in PBS for 48 hr. Sample sections (14 or 20 μm in thickness) were prepared on gelatin-coated glass slide with a cryostat (CM1520, Leica Microsystems Inc.).

An antigen retrieval method was used to label cells incorporated with BrdU as described previously (Obiorah et al., 2015). Sample sections were pretreated with 50%

formamide in 2X standard saline citrate (SSC) for 2 h at 65 °C, followed by 15 min in 2X SSC at room temperature, 30 min in 2N HCl at 37 °C, 10 min in 0.1 M borate buffer and rinsed in Tris-buffered saline (TBS) thrice, pH 7.3, at room temperature. After then, non-specific labeling was blocked with 5% goat serum and 0.3% Triton X-100 (Sigma) in TBS buffer for 60 min, and then incubated overnight at 4°C with a monoclonal rabbit anti-mouse antibody against BrdU (1:250, Sigma) and/or other primary antibody for rabbit-anti-Iba1 (1:1000, Wako Chemicals, 019-19741), donkey-anti-Iba1 (1:500, Abcam Inc ab5076), rabbit-anti-GFAP (1:500, Cell Signaling Technology 12389), rabbit-anti-NeuN (1:1000, Abcam Inc. ab104225), rabbit-anti-NG2 (1:500, Millipore Inc, AB5320), rabbit-anti-P2Y12 (1:500, Anaspec Inc. AS55043A), rabbit-anti-ki67 (1:200, Abcam Inc. ab 16667) for 24-48 hours. After primary antibody incubation, sections were rinsed in TBS and incubated for 60 min at RT with secondary antibodies (Alexa Fluor® 594: A-20185 or Alexa Fluor® 488: A-20181, Life Technologies). After rinses in TBS, the sections were mounted with Fluoromount-G (SouthernBiotech) and fluorescent images were obtained with a confocal microscope (LSM510, Zeiss).

The cell number was countered using ImageJ software (National Institutes of Health, Bethesda, MD). To quantify immunoreactivity profiles in the spinal cord, three to five L4–5 spinal cord sections per mouse from 4 mice were randomly selected for each group.

Spinal Cord Slice Preparation and 2-photon Imaging

Seven – nine week old adult mice were deeply anesthetized with isoflurane, and lumbosacral laminectomies were performed in an ice-cold chamber. Slice preparation

and 2-photon imaging were described previously (Eyo et al., 2014; Gu et al., 2015). The lumbosacral spinal cord was quickly removed and placed in ice-cold, sucrose-substituted artificial CSF saturated with 95% O_2 and 5% CO_2 (sucrose ACSF, in mM: sucrose, 234; KCl, 3.6; $CaCl_2$, 2.5; $MgCl_2$, 1.2; NaH_2PO_4, 1.2; $NaHCO_3$, 25; and D-glucose, 12). Transverse (300 μm) lumbar spinal cord slices were prepared in ice-cold sucrose ACSF using a vibratome. The slices were then maintained in a recovery chamber for 30 or more minutes and studied at room temperature (22–25°C) in regular ACSF equilibrated with 95% O_2 and 5% CO_2 (ACSF, in mM: NaCl, 125; KCl, 2.5; $CaCl_2$, 2; $MgCl_2$, 1, NaH_2PO_4, 1.25; $NaHCO_3$, 26; and D-glucose, 25, and sucrose added to make 300–320 mOsmol) before imaging.

Two-photon imaging experiments were conducted at room temperature with slices maintained in oxygenated regular ACSF with the same composition as mentioned above in a perfusion chamber at a flow rate of 2 mL/min. GFP-labeled microglia were imaged using a two-photon microscope (Scientifica) with a Ti:sapphire laser (Mai Tai; Spectra Physics) tuned to 900 nm for GFP-labeled microglia with a 40X water-immersion lens (0.8 NA; Olympus). The laser power was maintained at 25 mW or below. Microglia were imaged in between 40-100 μm of the spinal cord slice surface. Images were collected for ~ 200 minutes.

Quantitative RT-PCR

WT mice were sacrificed 7 days after SNT. Sham (spinal nerve uninjured) mice (n=3) were used as controls. The lumbar spinal cord was rapidly dissected and the ipsilateral spinal cord was divided into dorsal and ventral horn halves. We used the RNeasy

Minikit to extract mRNA after which 200 ng of purified mRNA was reverse-transcribed into cDNA using M-MLV (Promega). The mRNA levels for CCR2 and GAPDH were quantified with a Realplex2 real-time PCR system (Eppendorf) using SYBR Green PCR Master Mix (Applied Biosystems, Warrington, UK). All primers were designed using the NCBI Primer-BLAST program. GAPDH was used as the internal control for all the samples. The primer pair used are: CCR2 CCTGTCATTTATGCCTTTGTTG / GCTCACTCGATCTGCTGTCTC, GAPDH TGGTGAAGGTCGGTGTGAAC / GCTCCTGGAAGATGGTGATGG. Ratios of CCR2 to GAPDH mRNA were compared and analyzed.

Statistical Analysis

No statistical methods were used to predetermine sample sizes, but our sample sizes are similar to those reported in previous publications (Eyo et al., 2014; Gu et al., 2015). All data are expressed as mean ± S.E.M. Quantification of cells was done with ImageJ software for statistical analysis using unpaired 2-tailed Student's t-test. Behavioral data were analyzed by Student's t test (2 time point comparison) where the normality was tested. In certain cases, repeated-measures ANOVA followed by post-hoc Tukey's test was performed where the response to treatment was affected by two factors: time and genotype. For the cumulative anti-nociceptive effect of AraC, the area under the curve (AUC) of the time course during the entire observation period (7 days) were determined as the index of pain hypersensitivities. The criterion for statistical significance was $P < 0.05$.

Supplemental References

Eyo, U.B., Peng, J., Swiatkowski, P., Mukherjee, A., Bispo, A., and Wu, L.J. (2014). Neuronal Hyperactivity Recruits Microglial Processes via Neuronal NMDA Receptors and Microglial P2Y12 Receptors after Status Epilepticus. J Neurosci *34*, 10528-10540.

Gu, N., Eyo, U.B., Murugan, M., Peng, J., Matta, S., Dong, H., and Wu, L.J. (2015). Microglial P2Y12 Receptors Regulate Microglial Activation and Surveillance during Neuropathic Pain. Brain Behav Immun.

Gu, N., Niu, J.Y., Liu, W.T., Sun, Y.Y., Liu, S., Lv, Y., Dong, H.L., Song, X.J., and Xiong, L.Z. (2012). Hyperbaric oxygen therapy attenuates neuropathic hyperalgesia in rats and idiopathic trigeminal neuralgia in patients. Eur J Pain *16*, 1094-1105.

Hashimoto, M., Sun, D., Rittling, S.R., Denhardt, D.T., and Young, W. (2007). Osteopontin-deficient mice exhibit less inflammation, greater tissue damage, and impaired locomotor recovery from spinal cord injury compared with wild-type controls. J Neurosci *27*, 3603-3611.

Obiorah, M., McCandlish, E., Buckley, B., and DiCicco-Bloom, E. (2015). Hippocampal developmental vulnerability to methylmercury extends into prepubescence. Frontiers in neuroscience *9*, 150.

Wang, X., Cao, K., Sun, X., Chen, Y., Duan, Z., Sun, L., Guo, L., Bai, P., Sun, D., Fan, J.*, et al.* (2015). Macrophages in spinal cord injury: phenotypic and functional change from exposure to myelin debris. Glia *63*, 635-651.